Multinuclear, Multidimensional NMR Studies of *Anabaena 7120* Heterocyst Ferredoxin. Sequence-Specific Resonance Assignments and Secondary Structure of the Oxidized Form in Solution†

Young Kee Chae,‡,§ Frits Abildgaard,§ Ed S. Mooberry,§ and John L. Markley*,‡,§

Graduate Program in Biophysics and Department of Biochemistry, University of Wisconsin—Madison, 420 Henry Mall, Madison, Wisconsin 53706

Received October 4, 1993; Revised Manuscript Received December 2, 1993®

ABSTRACT: Sequence-specific assignments were determined for the diamagnetic proton resonances from recombinant *Anabaena 7120* heterocyst ferredoxin (M_r = 11 000) produced in *Escherichia coli*. Several samples selectively labeled with nitrogen-15 were prepared for use in two-dimensional heteronuclear multiple quantum coherence (HMQC) [Müller, L. (1979) *J. Am. Chem. Soc. 101*, 4481–4484] experiments. A sample uniformly labeled with nitrogen-15 was also prepared and used in two three-dimensional experiments: NOESY–HMQC and TOCSY–HMQC [Zuiderweg, E. R. P., & Fesik, S. W. (1989) *Biochemistry 28*, 2387–2391; Marion, D., Ikura, M., Tschudin, R., & Bax, A. (1989) *J. Magn. Reson. 85*, 393–399]. The sequential assignment strategy relied on the detection of ^{15}N-edited interresidue $^1H^{\alpha}_i$/$^1H^{N}_{i+1}$ NOE connectivities. Starting points and checks were provided by HMQC spectra of the selectively labeled samples. A sample doubly labeled with carbon-13 and nitrogen-15 was also prepared and used in three triple-resonance experiments: HNCA, HNCO, and HN(CO)CA [Ikura, M., Kay, L. E., & Bax, A. (1990) *Biochemistry 29*, 4659–4667; Kay, L. E., Ikura, M., Tschudin, R., & Bax, A. (1990) *J. Magn. Reson. 89*, 496–514]. The HNCA and HN(CO)CA spectra, which were used to confirm assignments from NOE connectivities, provided independent sequential assignments from spin couplings. Resonances from 18 residues were not seen in the diamagnetic region of the NMR spectrum. Several of these residues are very close to the [2Fe–2S] cluster, and their absence is explained by paramagnetic broadening and/or shifting. Other of these residues are located in a very flexible region, and the absence of their signals is attributed to exchange effects. Secondary structural features (four β-sheets and two α-helices) were determined purely on the basis of interresidue NOE connectivities. Structural information from NMR is compared to that from the X-ray structure of the same protein [Jacobson, B. L., Chae, Y. K., Markley, J. L., Rayment, I., & Holden, H. M. (1993) *Biochemistry 32*, 6788–6793] and from the related *Anabaena 7120* vegetative ferredoxin. Observed differences in local mobility and structure may be responsible for the differential specificity of the heterocyst and vegetative ferredoxins.

Nitrogen fixation is widespread among the cyanobacteria (Postgate, 1982; Stewart, 1980). In many members of this group, the process is aerobic. The rationale for this is that cyanobacteria, unlike photosynthetic bacteria, produce oxygen during photosynthesis. Most diazotrophic cyanobacteria are filamentous. Among the filamentous types, many possess specialized cells called heterocysts at intervals along the filament. The *Anabaena 7120* species belongs to this group. In these filamentous cyanobacteria, aerobic nitrogen fixation is restricted to heterocysts, which differentiate from vegetative cells upon the exhaustion of nitrogen in the medium. Heterocyst ferredoxin can be classified as a plant-type ferredoxin. It is a member of the [2Fe–2S] type of iron–sulfur proteins, which are present in virtually all organisms and in which the cluster is ligated to the protein by four cysteine residues. Heterocyst ferredoxin undergoes a one-electron redox reaction with a midpoint redox potential of –405 mV (Schrautemeier & Böhme, 1985; Böhme & Schrautemeier, 1987a). In the oxidized form, both iron atoms are Fe(III); in the reduced form, one iron atom remains Fe(III), but the other iron atom is changed to Fe(II). The physiological function of the heterocyst ferredoxin is to transfer one electron to the nitrogenase component II (Fe protein) as an immediate electron donor (Böhme & Schrautemeier, 1987b).

The heterocyst ferredoxin can be clearly distinguished from the vegetative ferredoxin from *Anabaena 7120*, with which it shares 52% sequence homology, by its biochemical and biophysical properties, including the isoelectric point, the midpoint redox potential, and the EPR spectrum (Böhme & Schrautemeier, 1987a). The heterocyst ferredoxin can transfer an electron to the nitrogenase, whereas the vegetative ferredoxin cannot. The relative inefficiency of the vegetative ferredoxin in transferring an electron to the nitrogenase can be attributed to its poorer interaction with that protein (Schrautemeier & Böhme, 1985). Since the X-ray structures of the two ferredoxins are very similar (Rypniewski et al., 1991; Jacobson et al., 1993), small unexplained differences in structure and/or flexibility from the vegetative ferredoxin must enable the heterocyst ferredoxin to interact efficiently with the nitrogenase.

† This work was supported by USDA/SEA Grant No. 9200684 and NSF Grant MCB-9215142. NMR studies were carried out at the National Magnetic Resonance Facility at Madison, which is supported by NIH Grant RR02301. Equipment in the NMR facility was purchased with funds from the NIH Biomedical Research Technology Program (Grant RR02301), the University of Wisconsin, the NSF Biological Instrumentation Program (Grant DMB-8415048), the NIH Shared Instrumentation Program (Grant RR02781), and the U.S. Department of Agriculture.

* Author to whom correspondence should be addressed.
‡ Graduate Program in Biophysics.
§ Department of Biochemistry.

® Abstract published in *Advance ACS Abstracts,* February 1, 1994.

0006-2960/94/0433-3287$04.50/0

NMR spectroscopy is the method of choice for studying the solution conformation and dynamic properties of biological macromolecules. Conventional two-dimensional NMR experiments such as DQF-COSY[1] (Rance et al., 1983), NOESY (Jeener et al., 1979), and TOCSY (Braunschweiler & Ernst, 1983) have been used for assignments of proton resonances and for structural determination of small proteins (<10 kDa). However, for larger proteins or for paramagnetic proteins of any size, such conventional NMR spectra are complicated by the spectral overlap of broad lines (Fesik & Zuiderweg, 1990). The instability of iron–sulfur proteins presents a further complication because denaturation of even a small fraction of the sample leads to the release of paramagnetic ions that relax the magnetization and severely broaden the NMR signals.

The present investigations of the heterocyst ferredoxin from *Anabaena 7120* employed one sample uniformly labeled with ^{15}N, several samples selectively labeled with ^{15}N, and one sample doubly labeled with ^{13}C and ^{15}N. A variety of NMR data sets was collected with these samples: two-dimensional heteronuclear correlation spectra, three-dimensional double-resonance spectra, and three-dimensional triple-resonance spectra. The basic assignment strategy relied on interresidue NOEs, but many sequential assignments were confirmed by triple-resonance data. Four-dimensional NMR experiments were attempted, but they were not successful owing to the low stability of the heterocyst ferredoxin.

We compare the present NMR results for the heterocyst ferredoxin with those for the vegetative ferredoxin (Oh & Markley, 1990), and we relate the solution structural information to the X-ray data for the same two proteins (Rypniewski et al., 1991; Jacobson et al., 1993). With the exception of one region, which may explain their functional differences, the solution structures of the two ferredoxins are very similar.

MATERIALS AND METHODS

Plasmid Construction and Purification of the Labeled Heterocyst Ferredoxin. The cloned structural gene for heterocyst ferredoxin (*fdx H*) (Böhme & Haselkorn, 1988) in a pUC plasmid (Böhme & Haselkorn, 1989) was subcloned into the overexpression vector pET-9a(–) [a slightly modified form of the original pET-9a vector (Novagen)] behind the T7 promoter by making use of two restriction sites: *Nhe*I and *Bam*HI. The resulting plasmid, in which the heterocyst ferredoxin gene is under the control of the T7 promoter, was named pKID. This plasmid was transformed into *E. coli* strain BL-21(DE3), which has the T7 RNA polymerase gene in its chromosome along with another plasmid, pLysS, which serves to suppress the basal level of expression of the heterocyst ferredoxin before induction. To label the protein uniformly with ^{15}N, $^{15}NH_4Cl$ was used in place of other nitrogen sources in the M9 medium. To label the protein uniformly with ^{13}C and ^{15}N, $^{15}NH_4Cl$ and [^{13}C]glucose were used, respectively, as the carbon and nitrogen sources. To label the protein selectively, ^{15}N-labeled amino acids were incorporated according to the recipes of Muchmore et al. (1989); however, a single *Escherichia coli* strain [BL21(DE3)] was used in place of the several auxotrophic strains. In most cases, the label did not migrate to other amino acids; exceptions are discussed below.

The inoculated culture was grown at 37 °C until the OD_{600} reached 1.0–1.2. Production of the heterocyst ferredoxin was initiated by adding IPTG. After 3 h of growth, the cells were harvested by centrifugation. The reconstitution procedure used was that described in Jacobson et al. (1992). The crude extract from the reconstitution step was first loaded onto a Q-Sepharose (Pharmacia) column (3 cm diameter × 10 cm length) and then eluted with a 0.2–0.6 M NaCl gradient. All of the brown fractions were pooled, concentrated, and loaded onto a G-50 (Pharmacia) column (3 cm diameter × 100 cm length). Normally, at this point (after the G-50 column), almost all of the brown fractions were at least 95% pure, as determined by the ratio of two absorbances measured at 276 and 422 nm [$A_{422}/A_{276} \geq 0.76$ for pure heterocyst ferredoxin (Böhme & Haselkorn, 1989)]. Pooled brown fractions that did not meet this criterion again were loaded onto the Q-Sepharose column and eluted with a 0.2–0.6 M NaCl gradient. The yield of purified heterocyst ferredoxin was approximately 20 mg/L of culture.

NMR Data Collection. NMR samples contained 4–5 mM heterocyst ferredoxin in 0.5 mL of 20 mM phosphate buffer (pH 7.5). The experiments required the observation of amide protons, so that the solvent contained 90% H_2O and 10% D_2O (for the lock signal).

All NMR data were collected at 25 °C, on either a Bruker AM-500 or a Bruker AM-600 spectrometer. NMR data were processed on Silicon Graphics workstations with FELIX (Hare Research, Inc.) software. ^1H chemical shifts were referenced to internal TSP (Cambridge Isotope Laboratories) at pH 7.5 and 25 °C. ^{15}N chemical shifts were referenced to external [^{15}N]acetylglycine by assuming that the ^{15}N resonance of [^{15}N]acetylglycine is at 120.0 ppm. ^{13}C chemical shifts were referenced to external [^{13}C]acetate by assuming that the methyl resonance of [^{13}C]acetate is at 24.5 ppm.

2D HMQC Experiments. Two proton carrier frequencies were used for HMQC (Müller, 1979) data collection. One was located at the center of the amide protons, and the other was at the water frequency. First, DANTE-type (Morris & Freeman, 1978) presaturation was applied for 1.5 s to suppress the H_2O resonance. The delay time used to create antiphase coherence was set to 4.5 ms. Quadrature detection in t_1 was accomplished by the TPPI method (Marion & Wüthrich, 1983). Typically, 128 or 256 t_1 increments were collected for each experiment. Nitrogen resonances were GARP-decoupled (Shaka et al., 1985) during the acquisition period. Each final 2D data matrix ($\omega_2 \times \omega_1$) contained 2048 × 512 points.

3D NOESY–HMQC Experiments. The principles and applications of the 3D NOESY–HMQC experiment have been described in detail (Kay et al., 1989; Zuiderweg & Fesik, 1989). 3D NOESY–HMQC data were recorded exclusively on a Bruker AM-600 spectrometer. A 10 000°$_x$–5000°$_y$ ^1H pulse was used at the end of each acquisition to achieve a steady state (Marion et al., 1989). DANTE-type presaturation was applied for 1.5 s to suppress the water resonance. After presaturation, two composite 180° pulses, separated by a delay (30 ms), were used to recover saturated α-proton resonances (SCUBA; Brown et al., 1988). The NOE mixing times in the two data sets were 100 and 120 ms, respectively. GARP decoupling was applied during t_1 (proton evolution) and t_3

[1] Abbreviations: COSY, correlated spectroscopy; DQC, double quantum coherence; DQF, double quantum filtered; HMQC, heteronuclear multiple quantum coherence; HNCA, correlation among amide proton, nitrogen, and α-carbon; HNCO, correlation among amide proton, nitrogen, and carbonyl carbon; HN(CO)CA, correlation among amide proton, nitrogen, and α-carbon via the carbonyl carbon; IPTG, isopropyl β-D-thiogalactoside; MBC, multiple bond correlation; NOESY, nuclear Overhauser effect spectroscopy; SBC, single-bond correlation; TOCSY, total correlation spectroscopy; TPPI, time proportional phase increment; TSP, 3-(trimethylsilyl)propionate-d_4.

(acquisition). The proton carrier was alternated between the water resonance and the center of the amide protons. The TPPI method was used to achieve quadrature detection in t_1. The States–TPPI (Marion et al., 1989; Clore & Gronenborn, 1991) method was used to achieve quadrature detection in t_2 (nitrogen evolution). The 3D data matrix ($\omega_1 \times \omega_2 \times \omega_3$) contained 256 (real) × 32 (complex) × 512 (real) data points. The two data sets with different mixing times were added together after they were fully processed to frequency domain spectra.

3D TOCSY–HMQC Experiments. 3D TOCSY–HMQC data were acquired as described by Clubb et al. (1991). DANTE-type presaturation and SCUBA pulses were used as above. Two mixing sequences were employed: WALTZ (Shaka et al., 1983) for data collected on the AM-600 instrument and DIPSI (Shaka et al., 1988) for data collected on the AM-500 instrument. On the AM-600, two WALTZ mixing times (29 and 44 ms) were used, respectively, in collecting two data sets that were added together after processing. The proton carrier was alternated as described above, and quadrature detection in t_1 was achieved by the TPPI method. On the AM-500, the proton carrier was fixed at the water resonance frequency, and a DIPSI-2 sequence was used with four mixing times: 38, 58, 78, and 98 ms. The four, time-domain data sets were added together and processed as one. Quadrature detection in t_1 was achieved by the States mode (States et al., 1982). The 3D data matrix contained 256 (real) × 32 (complex) × 512 (real) (AM-600) or 128 (complex) × 32 (complex) × 512 (real) (AM-500) data points. GARP decoupling was applied during t_1 and t_3.

3D Triple-Resonance Experiments. HNCA, HNCO, and HN(CO)CA (Ikura et al., 1990; Kay et al., 1990) spectra were collected on a Bruker AM-500 spectrometer that had been modified extensively (Mooberry et al., 1993). The proton carrier was fixed at the water resonance frequency. DANTE-type presaturation was used. The carbon carrier frequecies were set to 57.84, 173.13, and 55.21 ppm for the HNCA, HNCO, and HN(CO)CA experiments, respectively. The nitrogen carrier frequency was set to 120 ppm. The time-domain data sets had the following sizes: HNCO experiment, 55 (^{15}N, complex) × 64 (^{13}C′, complex) × 2048 (^{1}H, real); HNCA experiment, 33 (^{15}N, complex) × 64 (^{13}Cα, complex) × 2048 (^{1}H, real); and HN(CO)CA experiment, 49 (^{15}N, complex) × 64 (^{13}Cα, complex) × 2048 (^{1}H, real) points in t_1, t_2, and t_3, respectively. Quadrature detection in the carbon and nitrogen dimensions were achieved by the States–TPPI method. For the nitrogen dimension, constant-time evolution (Grzesiek & Bax, 1992) was used so that mirror image linear prediction processing (Zhu & Bax, 1990) could be applied. The final processed matrices contained 128 (ω_1) × 128 (ω_2) × 2048 (ω_3) real points.

RESULTS

The 2D HMQC data from selectively labeled samples were used to determine starting points for sequential assignments (example shown in Figure 1) and to confirm the correctness of sequential assignments. Samples labeled selectively with [^{15}N]glycine, -leucine, -valine, -alanine, or -lysine proved to be most useful for these purposes (other data not shown).

Assignment of α-Helical Segments. An α-helix is characterized by distinctive patterns of short-range NOEs: H^{α}_i/H^{N}_{i+3}, H^{N}_i/H^{N}_{i+2}, H^{α}_i/H^{N}_{i+2}, H^{α}_i/H^{N}_{i+4}, H^{β}_i/H^{N}_{i+1}, etc. (Wüthrich, 1986). Of these, the most important NOE connectivities are the first two, which correspond to distances in regular polyalanine α-helices of 3.4 and 4.2 Å, respectively, and H^{N}_i/H^{N}_{i+1}, which corresponds to a distance of 2.8 Å.

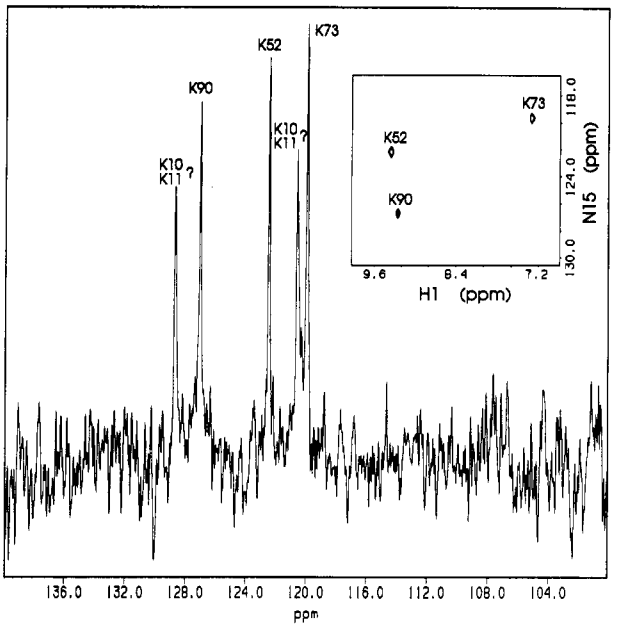

FIGURE 1: One-dimensional ^{15}N spectrum of [^{15}N]Lys-labeled *Anabaena 7120* heterocyst ferredoxin. Proton decoupling was used during the direct detection of ^{15}N. The inset shows the two-dimensional ^{1}H{^{15}N} HMQC spectrum of the same sample.

The presence of two α-helices in oxidized *Anabaena 7120* heterocyst ferredoxin was deduced from the 3D NMR data (Figures 2 and 3). One helix runs from Asp-28 to Glu-36, and the other runs from Glu-69 to Ala-76.

(1) Residues from Asp-28 to Glu-36. Gly-29 and Ala-30 were assigned sequentially with the help of the selectively labeled samples. Very strong NOE connectivities were detected between Gly-29-H^{α}/Ala-30-H^{N} and between Gly-29-H^{N}/Ala-30-H^{N}. H^{N}_i/H^{N}_{i+1} NOEs were found for the residues between Ala-30 and Ile-35 (Figure 2B). In addition, longer range, nonsequential NOEs were detected between certain H^{N}_i/H^{N}_{i+2} pairs. NOE connectivities were observed between Gly-29-H^{α}/Glu-31-H^{N}, Gly-29-H^{α}/Glu-32-H^{N}, and Ala-30-H^{α}/Asn-33-H^{N}, but not between other such pairs in this stretch; this suggests that the first half of the α-helix is tighter than the second half. The H^{α} of Asn-33 is not shown in Figure 2B, but it was detected in the TOCSY–HMQC spectrum. Glu-36 yielded a weaker H^{N}_i/H^{N}_{i+1} NOE peak, which may indicate that this residue marks the end of this helix.

(2) Residues from Glu-69 to Ala-76. The stretch from Glu-69 to Phe-75 showed strong H^{N}_i/H^{N}_{i+1} and H^{α}_i/H^{N}_{i+1} NOEs. Additional distances characteristic of an α-helix were indicated by H^{α}_i/H^{N}_{i+n} type NOE connectivities for Gln-70-H^{α}/Lys-73-H^{N}, Met-71-H^{α}/Gly-74-H^{N}, Gly-72-H^{α}/Gly-74-H^{N}, Met-71-H^{α}/Phe-75-H^{N}, and Gly-72-H^{α}/Phe-75-H^{N} and by H^{N}_i/H^{N}_{i+2} type NOE connectivities for Met-71-H^{N}/Lys-73-H^{N}, Gly-72-H^{N}/Gly-74-H^{N}, and Lys-73-H^{N}/Phe-75-H^{N}. A very weak amide-to-amide sequential NOE was found to connect Phe-75 and Ala-76, which may indicate that Ala-76 is the last residue in this helix.

Summary of Assignments and Helical Structure. Full ^{1}H, ^{13}C, and ^{15}N NMR assignments are presented in Table 1. Sequential and short-range NOE connectivities are given along with NH exchange results in Figure 4.

Assignment of β-Sheet Segments. The β-sheet has an influence on the chemical shifts of the α-protons in it; α-proton chemical shifts of residues in a β-sheet frequently are downfield of the water resonance. As seen in Table 1, many proton chemical shifts in the β-sheets are near or well below 5 ppm.

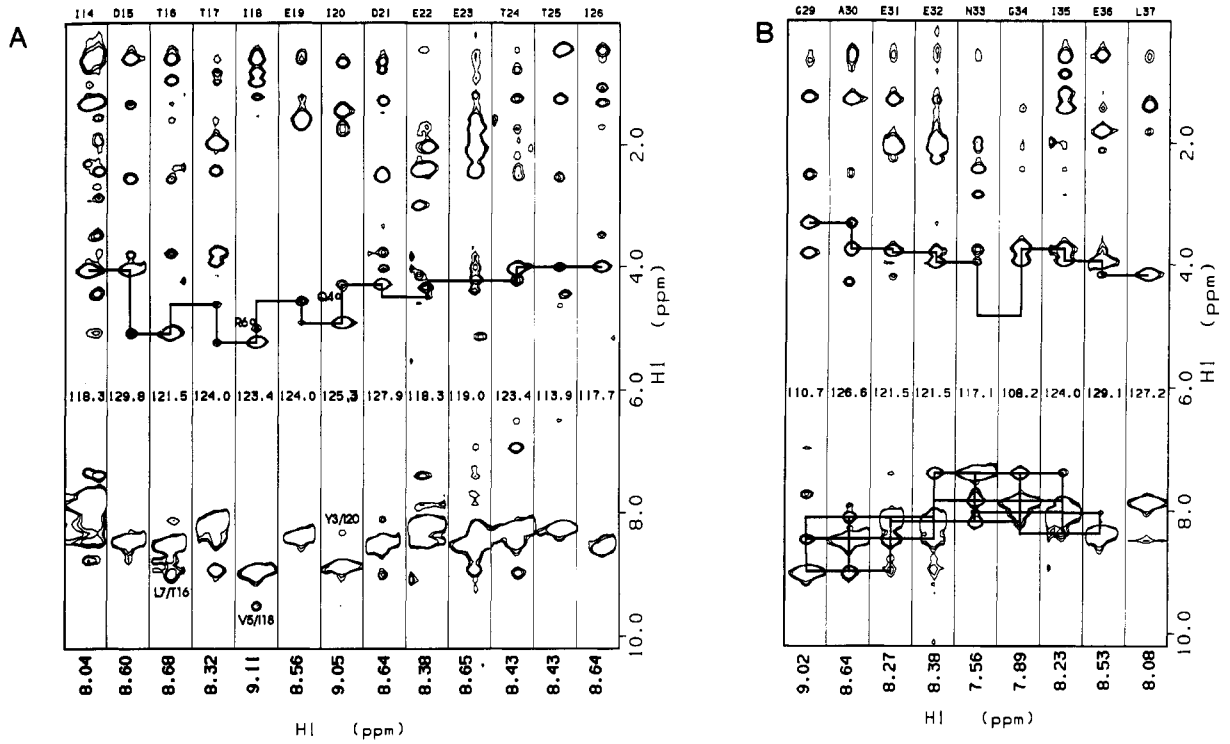

FIGURE 2: Series of strips selected from 2D ^1H–^1H slices of the 3D NOESY–HMQC spectrum. The assignment of each strip is given at its top. The nitrogen frequencies (derived from the 3D NOESY–HMQC spectrum) are given in the middle of the strips. (A) Sequential walk from Ile-14 to Ile-26. These residues form the second β-strand. (B) Sequential walk from Gly-29 to Leu-37. In addition to the H^{α}_i/H^N_{i+1} type NOE connectivities, H^N_i/H^N_{i+n} type connectivities are also shown. This panel contains data from the residues that form the first α-helix.

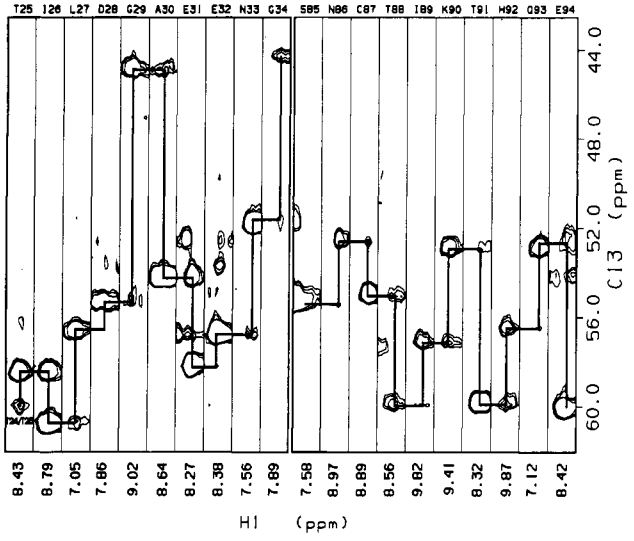

FIGURE 3: Series of strips selected from 2D slices of the 3D HNCA spectrum. Two interesting parts are shown. (Left) Sequential walk from Thr-25 to Gly-34. The sequential connectivity through Leu-27, which was missing in the double-resonance data, is evident here. (Right) Sequential walk from Ser-85 to Glu-94. The triple-resonance results allow the sequential connectivity to be extended to Glu-94; the necessary connectivities were missing in the double-resonance data.

The pattern of NOEs indicates the presence of four β-strands: two parallel β-strands are flanked by two antiparallel β-strands, which results in a mixed β-sheet structure (Figure 5). Residues 3–8 were found to act as the central strand. The parallel β-strand that interacts with it contains residues 86–91, and the antiparallel β-strand contains residues 16–20 (Figure 2A). Part of the 86–91 β-strand has a short antiparallel partner made up of residues 53 and 54. In the heterocyst ferredoxin, signals from first residue (Ala-1) were not detected in the ^1H–^{15}N data because the amine protons rapidly exchange with the solvent.

DISCUSSION

Assignment Strategy. Because of their paramagnetism, sequence-specific assignments of ferredoxins are difficult to obtain by conventional ^1H NMR methods. Novel strategies were developed by Oh and co-workers in their studies of the *Anabaena 7120* vegetative ferredoxin, the first ferredoxin for which extensive assignments were determined. The vegetative ferredoxin was labeled uniformly (to 26%) with ^{13}C, and the ^{13}C spin systems of the amino acid residues were mapped out by a 2D carbon–carbon double quantum experiment [^{13}C-{^{13}C} DQC; Oh et al., 1988]. The carbon connectivities were then extended to the protons by means of 2D single-bond and multiple-bond $^1H\{^{13}C\}$ correlations (Oh et al., 1989). The ^{13}C and ^1H spin systems were extended (over one to a few bonds) to neighboring ^{15}N atoms by collecting 2D $^1H\{^{15}N\}$ (Oh et al., 1989) and $^{13}C\{^{15}N\}$ data (Mooberry et al., 1989). The first experiment was performed on a ferredoxin sample labeled uniformly with nitrogen-15 (UL 98% ^{15}N), and the second experiment was performed on a double-labeled ferredoxin sample containing ^{15}N (UL 98%) and ^{13}C (UL 26%). Finally, sequential connectivities were deduced from sequential NOEs derived from standard NOESY spectra or from isotope-filtered 2D NOESY data (Oh & Markley, 1990).

The changes in assignment strategy instituted here for the heterocyst ferredoxin stem from (1) the difference in which the protein was produced (recombinant overproduction of the heterocyst ferredoxin in *E. coli* instead of direct isolation from *Anabaena 7120*, as was the case with the vegetative ferredoxin), and (2) recent developments in NMR experimentation, predominantly the introduction and refinement of 3D pulse sequences. Heterologous expression of the protein has led to a large increase in the yield per liter of culture and has made

Table 1: Chemical Shift Assignments for Oxidized *Anabaena 7120* Heterocyst Ferredoxin (pH 7.5, 25 °C)

	HN/N	Hα/Cα	Hβ	Hγ, Hδ, Hε	C′		HN/N	Hα/Cα	Hβ	Hγ, Hδ, Hε	C′
Ala-1					174.76	Ser-43					
Ser-2	8.97	4.74	2.63		174.66	Gly-44					
	122.1	51.95	3.48			Ser-45					
Tyr-3	8.48	4.96	2.10		172.43	Cys-46					
	120.9	54.39	3.12			Ser-47					
Gln-4	8.52	4.60	1.84	2.35	174.00	Ser-48					
	119.6	52.81	1.94	2.52		Cys-49					
Val-5	9.68	4.81	2.05	0.90	171.78	Val-50					173.35
	129.8	59.23				Gly-51	9.34				169.20
Arg-6	9.23	5.19	2.11		172.84		117.7	41.65			
	131.7	52.65				Lys-52	9.55	4.90	1.51		172.74
Leu-7	9.19	5.34	1.78	1.13	173.94		122.8	53.12			
	129.8	51.04				Val-53	9.68	3.99	2.14	0.60	174.46
Ile-8	8.64	4.95	1.62	0.91, 0.73	173.34		131.0	61.34		0.77	
	118.3	57.34				Val-54	8.81	4.11	1.95	0.87	174.15
Asn-9	8.68	3.99					128.5	61.00			
	121.5	57.55				Glu-55	7.58	4.52	1.97		175.11
Lys-10							119.0	54.03	2.20		
Lys-11					176.11	Gly-56	8.56	3.69, 4.62			170.72
Gln-12	7.49	4.32	1.22	2.00	172.33		111.3	41.86			
	115.2	52.28	1.68	2.28		Glu-57	8.02	4.65	1.48	2.05	173.09
Asp-13	7.86	4.27	2.51		172.88		118.3	52.63	1.75	2.15	
	119.0	53.45	3.12			Val-58	8.43	4.90			172.64
Ile-14	8.04	4.24	1.55	0.95, 0.83	174.86		113.3	56.47			
	118.3	58.56				Asp-59	9.25	5.03	2.55		173.40
Asp-15	8.60	5.26	2.76				121.5	51.42	2.84		
	129.8	52.29				Gln-60	9.27	5.72			175.17
Thr-16	8.68	4.82		1.18	169.90		126.0	51.39			
	121.5	58.57				Ser-61	8.43	4.24			173.60
Thr-17	8.32	5.44	3.94	1.06	172.23		118.3	61.11			
	124.0	59.96				Asp-62	9.17	4.78	2.62		174.66
Ile-18	9.11	4.76			171.47		120.2	53.32	2.91		
	123.4	56.81				Gln-63	8.43	4.81	1.94	2.26	173.65
Glu-19	8.56	5.11	1.84		174.46		123.4	54.16	2.04		
	124.0	53.12	1.99			Ile-64	7.73	4.05	1.33		
Ile-20	9.05	4.49	1.69	0.98, 0.87	172.79		131.7	51.58			
	125.3	58.56				Phe-65					174.66
Asp-21	8.64	4.70	2.70		174.56	Leu-66	10.55				176.20
	127.9	52.82					121.2	52.30			
Glu-22	8.38	4.35			174.76	Asp-67	8.60	4.76	2.62		174.77
	118.3	56.61					121.5	49.85	3.20		
Glu-23	8.65	4.41	1.96	2.27	173.55	Asp-68	8.37	4.35	2.60		177.92
	119.0	54.37	2.17	2.39			117.7	55.96			
Thr-24	8.43	4.19		1.42	169.65	Glu-69	8.32	4.11	2.20		178.30
	123.4	60.08					124.0	57.49	2.32		
Thr-25	8.43	4.19			175.45	Gln-70	9.09	4.19	2.55		178.61
	113.9	58.54					121.5	57.51			
Ile-26	8.79	3.70			175.80	Met-71	8.68	4.58			173.21
	117.7	60.79					119.6	57.86			
Leu-27	7.05				175.87	Gly-72	8.56	4.03			173.77
	115.8	56.61					111.3	44.64			
Asp-28	7.86	4.39			177.73	Lys-73	7.45	4.35	2.07	1.84, 1.59, 3.12	174.34
	119.0	55.41					119.6	54.73			
Gly-29	9.02	3.38, 3.87			174.46	Gly-74	7.67	3.54, 4.09			173.04
	110.7	44.97					105.0	42.54			
Ala-30	8.64	3.94	1.48		178.40	Phe-75	7.61	5.11	2.54		173.88
	126.6	54.21					120.2	58.22			
Glu-31	8.27	3.99	2.25		174.96	Ala-76	8.64	5.17	1.03		
	121.5	58.20					122.8	48.81			
Glu-32	8.38	4.16	2.13	2.30	175.17	Leu-77					
	121.5	56.82		2.43		Leu-78					
Asn-33	7.56	4.81	2.63		172.44	Cys-79					
	117.1	51.94	3.07			Val-80					172.33
Gly-34	7.89	3.76, 4.00			172.23	Thr-81	6.38	4.95			170.66
	108.2	44.30					117.7	60.64			
Ile-35	8.23	4.15	1.64	1.08, 0.77	174.36	Tyr-82	9.47	5.07	2.66		
	124.0	58.18					127.9	52.42			
Glu-36	8.53	4.35	2.00	2.30	173.70	Pro-83					174.15
	129.1	54.17	2.15			Arg-84	8.07	3.78			174.86
Leu-37	8.08	4.65	1.59				117.1				
	127.2	49.49				Ser-85	7.56	3.58	2.87		170.71
Pro-38							115.8	55.05			
Phe-39						Asn-86	8.89	5.31	2.51		176.63
Ser-40							119.6	52.67	2.85		
Cys-41						Cys-87	8.97	5.26	2.87		171.13
His-42							122.1	55.06			

Table 1 (Continued)

	HN/N	Hα/Cα	Hβ	Hγ, Hδ, Hε	C′		HN/N	Hα/Cα	Hβ	Hγ, Hδ, Hε	C′
Thr-88	8.56	5.37	3.86	1.06	171.62	Glu-94	8.42				
	118.3	59.93					125.3	60.08			
Ile-89	9.82	4.89	1.80	0.66	173.04	Pro-95		4.23	2.08		171.47
	129.8	57.16						63.65	0.78		
Lys-90	9.41	5.56	1.59	1.70, 2.06	175.71	Tyr-96	7.58	4.60	2.66		173.70
	127.2	53.02					115.2	55.12	3.10		
Thr-91	8.32	4.65			174.22	Leu-97	7.25	3.58	1.14		173.55
	115.2	59.93					122.1	54.03	1.59		
His-92	9.87	4.40	3.28		175.45	Ala-98	7.31	4.11	1.31		
	118.3	56.46					131.7	51.59			
Gln-93	7.12	4.73	1.56		174.08						
	111.3	53.00									

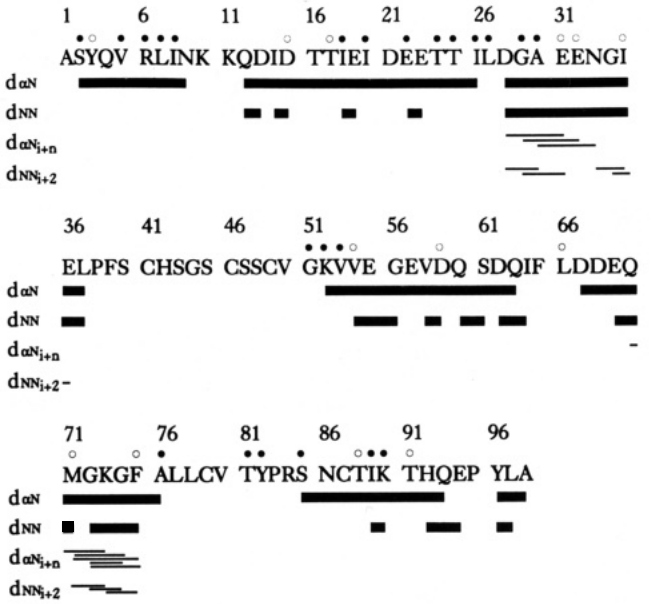

FIGURE 4: Primary sequence of *Anabaena 7120* heterocyst ferredoxin (Böhme et al., 1988) with a summary of observed sequential NOE connectivities and hydrogen exchange data. The open and filled circles above the sequence indicate slowly exchanging amide protons, as defined by the observation of a cross peak in the ^1H–^{15}N HMQC spectra taken 8 and 30 h after solvent exchange (H_2O to D_2O), respectively.

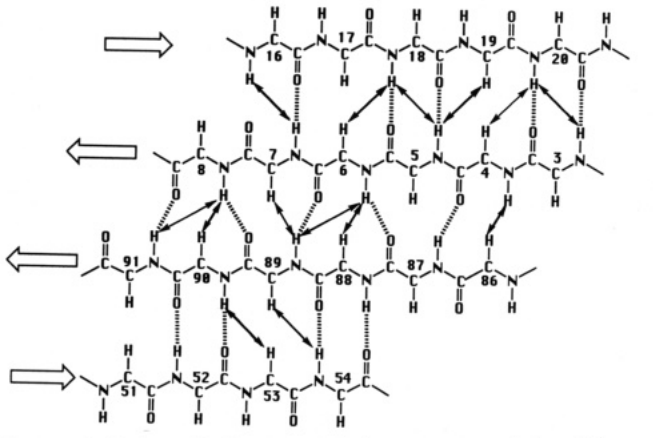

FIGURE 5: Schematic diagram of β-sheet structure deduced from the NOE results. One parallel β-strand is flanked by two antiparallel β-strands. Solid arrows represent the detected nonsequential NOEs. Putative hydrogen bonds are denoted by dotted lines.

it feasible to label the protein to 99% ^{13}C by growing the cultures on uniformly labeled glucose (instead of the $^{13}CO_2$ substrate used with the photosynthetic cyanobacterium). Overproduction of the protein in *E. coli* has also made it

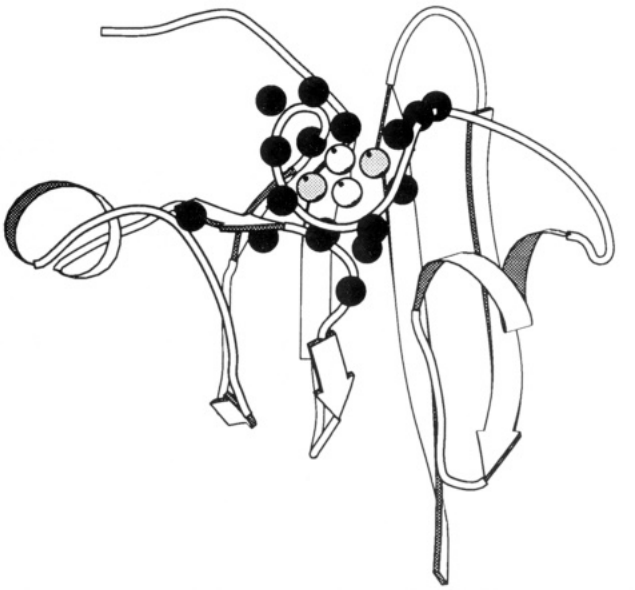

FIGURE 6: Molscript diagram (Kraulis, 1991) of the X-ray structure of the *Anabaena 7120* heterocyst ferredoxin. Filled spheres represent the positions of backbone nitrogen atoms whose signals are missing in 2D and 3D spectra. Open and shaded spheres represent the irons and sulfurs of the [2Fe–2S] cluster.

possible to label the protein selectively by feeding labeled amino acid residues as precursors.

Paramagnetic Effects. As was the case with *Anabaena 7120* vegetative ferredoxin (Oh & Markley, 1990), multinuclear, multidimensional approaches failed to reveal the full spin systems of several residues in the heterocyst ferredoxin (Figure 6). In the vegetative ferredoxin, the missing signals corresponded to residues with hydrogens in close proximity (about 7 Å) to the [2Fe–2S] cluster (Oh & Markley, 1990). Residues whose resonances were totally missing in the 3D NOESY–HMQC (Figure 2) and TOCSY–HMQC (not shown) spectral data for the heterocyst ferredoxin were Leu-27, Phe-39, Ser-40, Cys-41, His-42, Ser-43, Gly-44, Ser-45, Cys-46, Ser-47, Ser-48, Cys-49, Val-50, Phe-65, Leu-77, Leu-78, Cys-79, and Val-80. Residues whose resonances were only partially observed were Ile-26, Asp-28, Gly-51, Ile-64, Leu-66, Thr-81, and Glu-94. Some resonances could be assigned to these residues through NOE connectivities to adjacent amino acids or from other information: for example, the H^α and H^N resonances of Asp-28 were assigned with the help of NOE connectivities. The amide proton resonances of Gly-51 and Leu-66 were assigned tentatively on the basis of their chemical shifts in the spectra of samples selectively labeled with glycine and leucine. These assignments were confirmed by sequential, triple-resonance spin–spin connectivities to their neighboring residues (Leu-27, Gly-51, and Leu-66). This

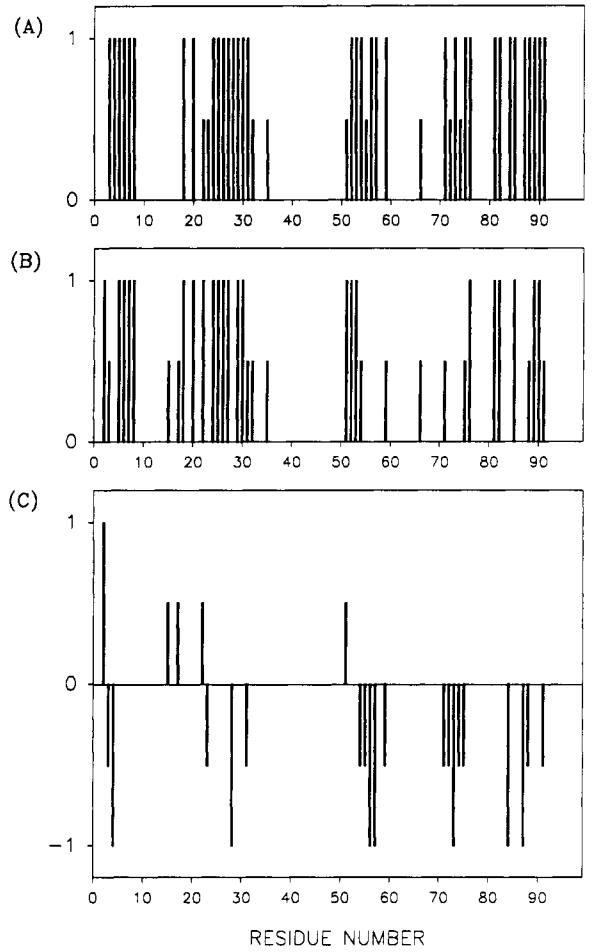

FIGURE 7: Schematic representation of regions in which amide hydrogen exchange is protected. Residues with amide exchange half-times of longer than 30 h are represented by bars of height 1.0, and those with half-times between 8 and 30 h are represented by bars of height 0.5. The remaining residues either have exchange half-times of less than 8 h or correspond to prolines or unassigned residues. (A) *Anabaena 7120* vegetative ferredoxin. (B) *Anabaena 7120* heterocyst ferredoxin. (C) Difference in protection between the two proteins (heterocyst − vegetative). Bars are shown only for residues for which exchange rates were determined in both proteins.

shows that triple-resonance experiments, which employ efficient one-bond couplings, can extend the number of assignments in paramagnetic proteins beyond those accessible by the methods used earlier. Figure 3A shows the connectivity through Leu-27, and Figure 3B shows the connectivity up to Glu-94.

Proline Residues. Resonances of one of the three proline residues were partially identified (Pro-95). The two other prolines (Pro-38 and Pro-83) seemed to be affected by the paramagnetic [2Fe–2S] cluster, and resonances from those residues were not identified.

Structural Comparisons of Anabaena 7120 Heterocyst and Vegetative Ferredoxins in Solution. (1) Comparison of Hydrogen Exchange Data. Figure 7 shows a qualitative comparison of the amide proton exchange rates of vegetative and heterocyst ferredoxins. The vegetative ferredoxin (Figure 7A) has more protected amide protons than the heterocyst ferredoxin (Figure 7B). This is seen clearly in Figure 7C, which indicates the difference in protection. Thus, the vegetative ferredoxin appears to be more rigid overall than the heterocyst ferredoxin. In our experience, the heterocyst ferredoxin is less stable in solution than the vegetative ferredoxin. Moreover, the heterocyst ferredoxin has proved to be more difficult to crystallize than the vegetative one (B. L. Jacobson, personal communication). These facts can be explained by the greater flexibility of the heterocyst ferredoxin.

An interesting local difference is found at residues 71–75, which form the second helix. In the vegetative ferredoxin, residues 68–76 form a loose helix, as indicated by uneven amide proton exchange rates (Oh & Markley, 1990). In the heterocyst ferredoxin, the amide protons of Met-71 and Phe-75 are partially protected and that of Ala-76 is more fully protected from exchange. All other amide protons exchange very rapidly with solvent protons. The results show that the 69–76 α-helix in both ferredoxins is less rigid than the 29–36 α-helix and that the 69–76 helix is less stable in the heterocyst ferredoxin than the vegetative.

(2) Comparison of NOE Data. In the vegetative ferredoxin, the first helix (residues 25–32) was well-defined by NOEs (Oh & Markley, 1990). In the spectra of the heterocyst ferredoxin, the side-chain resonances of Ile-26 and Asp-28 were broadened, presumably by the [2Fe–2S] cluster, but they could be assigned from sequential NOEs. Signals from Leu-27 were missing in the 3D ^{15}N-NOESY–HMQC and ^{15}N-TOCSY–HMQC data. These obstacles limited the determination of the first helix.

In the vegetative ferredoxin, NOEs between Thr-91-H$^{\alpha}$/Gly-51-H$^{\alpha}$ and between Gln-91-H^{N}/Lys-52-H^{N} demonstrated that the antiparallel β-sheet includes residues 51–54. Our data for the heterocyst ferredoxin do not include H$^{\alpha}$/H$^{\alpha}$ NOEs, but do include H^{N}/H^{N} NOEs. Thus, the lack of an observed Gln-92-H^{N}/Lys-52-H^{N} NOE for the heterocyst ferredoxin is significant. It may be missing because of the greater flexibility of the heterocyst ferredoxin near the active-site [2Fe–2S] cluster. This flexibility might explain why the heterocyst ferredoxin can bind both to nitrogenase and to FNR (ferredoxin NADP^{+} reductase), whereas the vegetative ferredoxin can bind only to FNR (Schrautemeier & Böhme, 1985; Böhme & Schrautemeier, 1987b).

(3) Comparison of the α-Proton Chemical Shifts of Vegetative and Heterocyst Ferredoxins. The chemical shifts of the α-protons of the two ferredoxins are compared in Figure 8A. This comparison indicates larger structural differences in the amino-terminal half of the protein than in the carboxyl half. Wishart et al. (1992) have developed a chemical shift index that provides good empirical correlations between NMR chemical shifts and secondary structure. The basis for this analysis is the finding that α-protons in α-helices experience an upfield shift, whereas those in β-sheets experience downfield shifts. Chemical shift indices were constructed for the α-protons of the vegetative and heterocyst ferredoxins (Figure 8BC) according to the procedure of Wishart et al. (1992). The chemical shift index is interpreted as follows (Wishart et al., 1992): Any dense grouping of four or more '−1's not interrupted by a '1' is an α-helix. Any dense grouping of four or more '1's not interrupted by a '−1' is a β-strand. All other regions are designated as coil. Regions 2–8, 14–20, 52–60, and 86–91 in both proteins are identified by the chemical shift index as β-sheet. This conclusion is consistent with all of the NOE results, with the exception of the third segment (52–60) which is longer than that deduced from the NOE data (Figure 5). As discussed below, the longer β-sheet is found in the X-ray structure. The chemical shift index identifies residues 28–36 as α-helix, as indicated by NOEs (Figure 4). However, whereas the NOE data show that residues 69–76 are helical, only residues 68 and 74 in this stretch have chemical shift indices of 1. Here the chemical shift index results are corroborated by hydrogen exchange data (Figures 4 and 7), which indicate that the amide protons

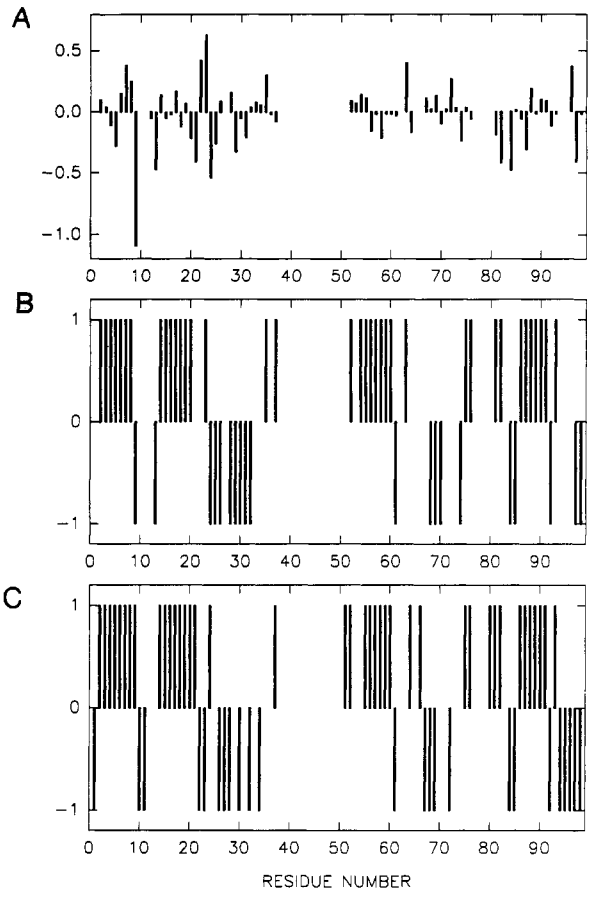

FIGURE 8: (A) α-Proton chemical shift difference between *Anabaena 7120* vegetative and the heterocyst ferredoxins. The difference was normalized to take sequence difference into account (see text). (B) Chemical shift index (Wishart et al., 1992) of the heterocyst ferredoxin. (C) Chemical shift index of the vegetative ferredoxin.

in this stretch readily exchange with solvent (more so for the heterocyst ferredoxin than for the vegetative ferredoxin).

Flexible Regions. Signals from Lys-10 and Lys-11 were not detected in the 3D NOESY–HMQC or TOCSY–HMQC experiments, and the 2D HMQC spectrum of the sample selectively labeled with [^{15}N]Lys showed only three peaks: Lys-52, Lys-73, and Lys-90 (Figure 1). However, the ^{15}N spectrum of the same sample (Figure 1) showed five peaks. The two ^{15}N peaks corresponding to those not detected in the HMQC experiment (Lys-10 and Lys-11) had lower intensity than the other three. This suggests that Lys-10 and Lys-11 are in a flexible region. By contrast, in the vegetative ferredoxin, these residues are part of a β-turn, and residues 10–14 show very strong H^N/H^N NOE connectivities (Oh & Markley, 1990). These facts may explain the major chemical shift differences between two proteins in the first half of the sequence (Figure 8A).

Comparison of NMR and X-ray Results. The increase in mobility at Lys-10 in the heterocyst ferredoxin as compared to the vegetative ferredoxin can be explained in terms of the X-ray structures of these proteins. In the vegetative ferredoxin (Rypniewski et al., 1990), Glu-10 is involved in a hydrogen bond to Lys-93. In the heterocyst ferredoxin, these residues are Lys-10 and Gln-93, and although one might have expected that the residue would still interact since the changes are partially compensatory, the X-ray structure shows that Lys-10 hydrogen bonds to the side chain of Asp-59 in a symmetry-related molecule. The latter interaction, which results from crystal packing, would not be present in solution. Apparently, Lys-10 is prevented from interacting with Gln-93 by the intervention of Lys-90 (Jacobson et al., 1993).

In the X-ray structure of the heterocyst ferredoxin, residues 10–13 form a type I turn. If this region is also a turn in the solution, it should show characteristic NOE connectivities. The vegetative ferredoxin exhibits strong H^N_i/H^N_{i+1} type NOEs connecting this region, which are in agreement with the X-ray result. The heterocyst ferredoxin, however, exhibits H^N_i/H^N_{i+1} type NOEs only between Gln-12 and Asp-13. The lack of such NOEs for Lys-10 and Lys-11 suggests that the type I turn at residues 10–13 seen in the X-ray structure either is not fully formed or is unstable in solution. In Figure 8A, a large chemical shift difference stands out at residue 9, which is consistent with the increased flexibility of residues 10–11 in solution. The flexibility may also influence the neighboring residues and may explain the more upfield α-proton chemical shift of Asn-9. The flexibility of residues 10 and 11 may cause fraying at the end of the first β-strand; this would explain the chemical shift of Asn-9, which is not characteristic of a β-sheet (Figure 8).

The chemical shift differences in the C-terminal residues of the two ferredoxins (Figure 8A) are also consistent with X-ray data. The X-ray structures (Jacobson et al., 1993) reveal structural differences between the two ferredoxins at the three C-terminal residues; these are attributed to Pro-95 in the heterocyst ferredoxin (residue 95 is Glu in the vegetative ferredoxin). This proline promotes a tight type I turn at residues 94–97 in the heterocyst ferredoxin, whereas a helical turn is present at residues 94–98 in the vegetative ferredoxin. The rather large chemical shift difference at 80–85 can be interpreted in terms of the chemical shift index: Because they are more downfield shifted, these residues seem to have more β-strand or extended structural character in the vegetative ferredoxin than in the heterocyst ferredoxin. Since these residues are also close to the [2Fe–2S] cluster, the structural differences may play a functional role.

According to the X-ray structure (Jacobson et al., 1993), the heterocyst ferredoxin contains two α-helices (26–31 and 68–72) and seven β-strands (1–9, 14–21, 51–53, 57–59, 75–77, 81–83, and 87–91). According to the NOE data (Figure 4), however, the secondary structure consists of two α-helices (28–36 and 69–76) and four β-strands (3–8, 16–20, 53–54, and 86–91) (Figure 5). The X-ray and NMR data are mutually consistent, except for the first helix and the short β-strands. NMR evidence for a helix at residues 32–36 comes from chemical shift index data (Figure 8) and from H^N_i/H^N_{i+2} NOEs. However, H^α_i/H^N_{i+3} NOEs at Gly-34 and Glu-36, which are expected for an α-helix, are absent, and amide hydrogen exchange in this region is rapid. Thus, residues 32–36 may not form a true α-helix in solution. The observed NOEs do not provide evidence for β-sheet at residues 57–59, 75–77, and 81–83. On the other hand, the chemical shift index diagram (Figure 8) shows a long stretch of 1's at 54–60 and short stretches of 1's at 75–76 and 81–82, which are consistent with the X-ray structure. When these data are taken into consideration, the β-sheet observed by NMR is quite similar to that found in the X-ray structure. (Chemical shift data are unavailable for Leu-77, which was affected by the paramagnetic cluster, or for residue 83, which is proline.)

Future Prospects. Work is in progress to identify the remaining unassigned hyperfine and motionally broadened signals. The present results lay the groundwork for solution studies of heterocyst ferredoxin mutants and for the investigation of the mechanism of interaction of heterocyst ferredoxin with the iron protein of nitrogenase.

ACKNOWLEDGMENT

We thank Dr. A. S. Edison for assistance with NMR instrumentation and Dr. J. F. Wang for useful discussions. The cloned *Anabaena 7120* heterocyst ferredoxin gene was kindly provided by Dr. Herbert Böhme.

REFERENCES

Böhme, H., & Schrautemeier, B. (1987a) *Biochim. Biophys. Acta 891*, 1–7.

Böhme, H., & Schrautemeier, B. (1987b) *Biochim. Biophys. Acta 891*, 115–120.

Böhme, H., & Haselkorn, R. (1988) *Mol. Gen. Genet. 214*, 278–285.

Böhme, H., & Haselkorn, R. (1989) *Plant Mol. Biol. 12*, 667–672.

Braunschweiler, L., & Ernst, R. R. (1983) *J. Magn. Reson. 53*, 521–528.

Brown, S. C., Weber, P. L., & Müller, L. (1988) *J. Magn. Reson. 77*, 166–169.

Clore, G. M., & Gronenborn, A. M. (1991) *Prog. Nucl. Magn. Reson. Spectrosc. 23*, 43–92.

Clubb, R. T., Osborne, T. C., & Wagner, G. (1991) *Biochemistry 30*, 7718–7730.

Fesik, S. W., & Zuiderweg, E. R. P. (1990) *Q. Rev. Biophys. 23* (2) 97–131.

Grzesiek, S., & Bax, A. (1992) *J. Magn. Reson. 96*, 432–440.

Ikura, M., Kay, L. E., & Bax, A. (1990) *Biochemistry 29*, 4659–4667.

Jacobson, B. L., Chae, Y. K., Böhme, H., Markley, J. L., & Holden, H. M. (1992) *Arch. Biochem. Biophys. 294*, 279–281.

Jacobson, B. L., Chae, Y. K., Markley, J. L., Rayment, I., & Holden, H. M. (1993) *Biochemistry 32*, 6788–6793.

Jeener, J., Meier, B. H., Bachmann, P., & Ernst, R. R. (1979) *J. Chem. Phys. 71* 4546–4553.

Kay, L. E., Marion, D., & Bax, A. (1989) *J. Magn. Reson. 84*, 71–84.

Kay, L. E., Ikura, M., Tschdin, R., & Bax, A. (1990) *J. Magn. Reson. 89*, 496–514.

Kraulis, P. J. (1991) *J. Appl. Crystallogr. 21*, 67–71.

Marion, D., & Wüthrich, K. (1983) *Biochem. Biophys. Res. Commun. 113*, 967–974.

Marion, D., Ikura, M., Tschdin, R., & Bax, A. (1989) *J. Magn. Reson. 85*, 393-399.

Mooberry, E. S., Oh, B.-H., & Markley, J. L. (1989) *J. Magn. Reson. 85*, 147–149.

Mooberry, E. S., Abildgaard, F., & Markley, J. L. (1993) *Methods Enzymol.* (in press).

Morris, G. A., & Freeman, R. (1978) *J. Magn. Reson. 29*, 433–462.

Muchmore, D. C., McIntosh, L. P., Russell, C., B., Anderson, D. E., & Dahlquist, F. W. (1989) *Methods Enzymol. 177*, 44–73.

Müller, L. (1979) *J. Am. Chem. Soc. 101*, 4481–4484.

Oh, B.-H., & Markley, J. L. (1990) *Biochemistry 29*, 3993–4004.

Oh, B.-H., Westler, W. M., Darba, P., & Markley, J. L. (1988) *Science 240*, 908–911.

Oh, B.-H., Westler, W. M., & Markley, J. L. (1989) *J. Am. Chem. Soc. 111*, 3083–3085.

Oh, B.-H., Mooberry, E. S., & Markley, J. L. (1990) *Biochemistry 29*, 4004–4011.

Postgate, J. R. (1982) *The Fundamentals of Nitrogen Fixation*, Cambridge University Press, Cambridge, UK.

Rance, M., Sørensen, O. W., & Ernst, R. R. (1983) *J. Am. Chem. Soc. 104*, 6800–6801.

Rypniewski, W. R., Breiter, D. R., Benning, M. M., Wesenberg, G., Oh, B.-H., Markley, J. L., Rayment, I., & Holden, H. M. (1991) *Biochemistry 30*, 4126–4131.

Schrautemeier, B., & Böhme, H. (1985) *FEBS Lett. 184* (2), 304–308.

Shaka, A. J., Keeler, J., Frenkiel, T., & Freeman, R. (1983) *J. Magn. Reson. 52*, 335–338.

Shaka, A. J., Barker, P. B., & Freeman, R. (1985) *J. Magn. Reson. 64*, 547–552.

Shaka, A. J., Lee, C. J., & Pines, A. (1988) *J. Magn. Reson. 77*, 274–293.

States, D. J., Haberkorn, R. A., & Ruben, D. J. (1982) *J. Magn. Reson. 48*, 286–292.

Stewart, W. D. P. (1980) *Annu. Rev. Microbiol. 34*, 497–536.

Wishart, D. S., Sykes, B. D., & Richards, F. M. (1992) *Biochemistry 31*, 1647–1651.

Wüthrich, K. (1986) *NMR of Proteins and Nucleic Acids*, Wiley, New York.

Zhu, G., & Bax, A. (1990) *J. Magn. Reson. 90*, 405.

Zuiderweg, E. R. P., & Fesik, S. W. (1989) *Biochemistry 28*, 2387–2391.